

# Automatic Vertebrae Segmentation in Fluoroscopic Images for Electrophysiology

Sabrina Reiml, Tanja Kurzendorfer, Daniel Toth, Peter Mountney,  
Stefan Steidl, Alexander Brost, and Andreas Maier

**Abstract**—Worldwide, heart failure affected about 26 million people in 2014. The treatment is mostly done minimally invasively, in particular when pharmacotherapy fails. As fluoroscopic images provide little functional or anatomical information of the heart, most often pre-operative magnetic resonance imaging data is used, to provide additional information. The 3-D data needs to be fused with the fluoroscopic images. Therefore, an accurate 2-D/3-D registration is necessary. This can be achieved by registering the bones in fluoroscopic images with the bones in magnetic resonance imaging data. However, a special bone magnetic resonance scan is needed. In this paper, we propose a learning based approach in combination with an active contour for the segmentation of vertebrae in fluoroscopic images. After preprocessing the fluoroscopic images, a random forest classifier is trained to extract the vertebrae. The resulting probability map is used to initialize an active contour approach for the segmentation of the vertebrae. The proposed method was evaluated on 12 fluoroscopic data sets and compared to a gold standard annotation obtained from a clinical expert. This comparison yielded a mean Dice coefficient of  $0.80 \pm 0.07$  and a vertebrae detection rate of 86 %.

**Index Terms**—segmentation, bones, vertebrae, fluoroscopic images, feature extraction, classification, machine learning, active contour.

## I. INTRODUCTION

IN 2014, about 26 million people suffered from heart failure (HF) [1]. The treatment is mostly done minimally invasively by implantation of a pacemaker, in particular when pharmacotherapy fails [2]. However, fluoroscopic images provide little functional or anatomical information to the cardiologist. Recent examples have demonstrated the use of magnetic resonance X-ray fusion for the guidance of implanting a pacemaker-like device [3]. Most commonly, pre-operative magnetic resonance imaging (MRI) data is acquired for diagnosis and treatment planning, as MRI data provides important information about function and viability of the heart muscle [4]. This data can then be fused with the fluoroscopic images during the intervention. Therefore, an accurate 2-D/3-D registration between the fluoroscopic images and MRI data is needed [5]. Currently, there are two main approaches for the registration: (a) fully manual registration [6], (b) fiducial marker based manual registration [7], and (c) automatic soft tissue-based approach using contrast agent and adjacent

S. Reiml, T. Kurzendorfer, S. Steidl and A. Maier are with the Department of Computer Science, Pattern Recognition Lab, Friedrich Alexander-University Erlangen-Nuremberg, Erlangen, Germany.

D. Toth is with King's College London.

P. Mountney and A. Brost are with Siemens Healthineers.

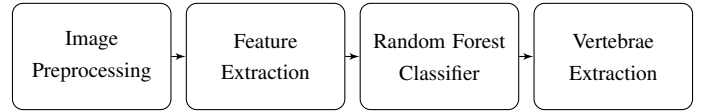


Fig. 1: Overview of the segmentation pipeline.

anatomical structures [8]. In this paper, we propose to register the vertebrae in the fluoroscopic image with the bones in the MRI. The output is the probability of a pixel belonging to a vertebra. To get the bones from the MRI, a special MRI scan needs to be acquired, where the bones are well visible. In this paper, we present the first step of the 2-D/3-D registration – the segmentation of the vertebrae in fluoroscopic images.

## II. SEGMENTATION OF THE VERTEBRAE

The segmentation pipeline consists of four steps, which are described in the next sections. After the preprocessing step, features are extracted and classified. In the end, the vertebrae are segmented using an active contour approach. An overview of the pipeline is depicted in Fig. 1.

### A. Image Preprocessing

The first step of the vertebrae segmentation in fluoroscopic images is preprocessing. The goal of preprocessing is to remove disturbing structures, noise, and to preserve the edges of the vertebrae. A fluoroscopic image is a digital video of low dose X-ray frames, i.e. acquired during an intervention with a C-arm system. An example for the first frame of an input fluoroscopic sequence, where the vertebrae will be segmented, is depicted in Fig. 2 (a). As a sequence of frames is acquired, there will be moving parts in the data set, i.e. a catheter, as depicted in Fig. 2 (a). To remove moving structures, background subtraction is performed [9]. Therefore, the maximum intensity algorithm is used [10]. The method takes for each pixel the maximum intensity from all frames, the result is depicted in Fig. 2 (b). Afterwards, bilateral filtering is performed on the background subtracted image to denoise the image and to preserve the edges of the vertebrae, see Fig. 2 (c) [11].

### B. Feature Extraction

In the second step, 30 features are extracted from the preprocessed image. The aim is to get features, which describe the vertebrae well. The extracted features are the intensity,

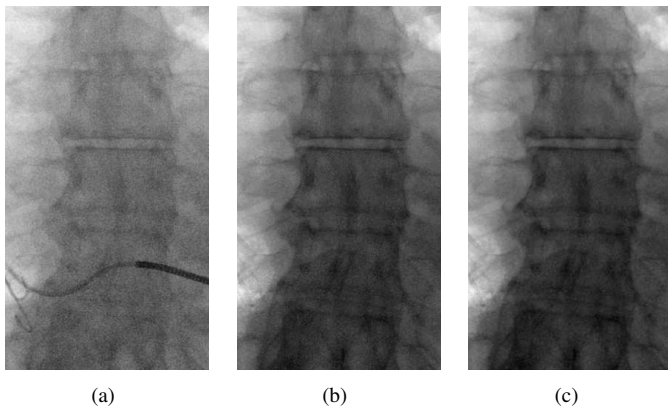


**Fig. 2:** Visualization of the first frame of the input fluoroscopic image and the two preprocessing steps: (a) The input image contains a moving catheter. (b) To remove moving parts, the maximum intensity algorithm is applied. (c) To strengthen the edges of the vertebrae and to denoise the image, bilateral filtering is used.

gradient in x- and in y-direction, magnitude of the gradients, histogram of oriented gradients, local binary pattern, and 24 features from the gray level co-occurrence matrix (GLCM) [12]. The GLCM is calculated using a patch size of  $5 \times 5$ , distances of 1 and 2, and orientations of  $0^\circ$  and  $90^\circ$ . From each of them the contrast, dissimilarity, homogeneity, angular second moment, energy, and correlation are computed.

### C. Random Forest Classifier

In the third step, a random forest classifier is trained [13]. The training of the classifier is based on ground truth annotations from which positive as well as negative samples are extracted. The output is the probability of a pixel belonging to a vertebra. An example of the resulting probability map is depicted in Fig. 3 (a). The probability ranges from blue to red, where blue denotes that the pixel is classified 0% as bone, and red denotes that the pixel is classified 100% as bone.

### D. Vertebrae Extraction

In the fourth step, the inverted preprocessed image and the probability map are added up to strengthen the bones. From this combined image, the pixel values are projected column- and row-wise. An example is depicted in Fig. 3 (b). From the column-wise projection (red), the x-coordinate of the vertebra is computed. With the row-wise projection (blue), at least one intervertebral disc (dotted light blue region) can be found robustly. Then the center of the neighboring vertebrae can be computed. In each of the detected centers, a morphological active contour is started, to determine the boundary of the vertebrae [14]. From these vertebrae segmentations, the next vertebrae centers are determined automatically. In the end, the contours are smoothed by dilation. The final result of the vertebrae segmentation is illustrated in Fig. 3 (c), where the gold standard annotation is green and the segmentation result red.

## III. EVALUATION AND RESULTS

The automatic segmentation of the vertebrae was evaluated on 12 clinical fluoroscopic images. The data was acquired with an Artis zee biplane system (Siemens Healthcare GmbH, Forchheim, Germany). Gold standard annotations were provided by one clinical expert. The segmentation result was evaluated with a leave-one-out cross-validation using the Dice coefficient (DC) and the detection rate of the vertebrae. The DC, ranging from 0 to 1, is a quantitative measure for the segmentation quality, as it measures the proportion of true positives in the segmentation. A perfect overlap correlates to 1. The segmentation resulted in a mean DC of  $0.80 \pm 0.07$ , where the best segmentation result had a DC of 0.87 and the worst a DC of 0.67. An overview is depicted in Table I. A vertebrae detection rate of 86% was achieved. Vertebrae at the boundary of the image, which are only partially visible, i.e. less than 50%, were not considered.

Dice Coefficient	
Mean $\pm$ Std.	$0.80 \pm 0.07$
Best Result	0.87
Worst Result	0.67

TABLE I: Evaluation results for the vertebrae segmentation using the Dice coefficient.

## IV. DISCUSSION AND CONCLUSION

Heart failure is most commonly treated minimally invasively. An accurate registration between the pre-operative MRI and the fluoroscopic data is needed. In this paper, we provide the first step of the registration pipeline, a novel method for segmenting vertebrae in fluoroscopic images. The segmented vertebrae in fluoroscopic images can be registered with the segmented bones from MRI data. In the course of this work, it has been shown that simple features can be used for the

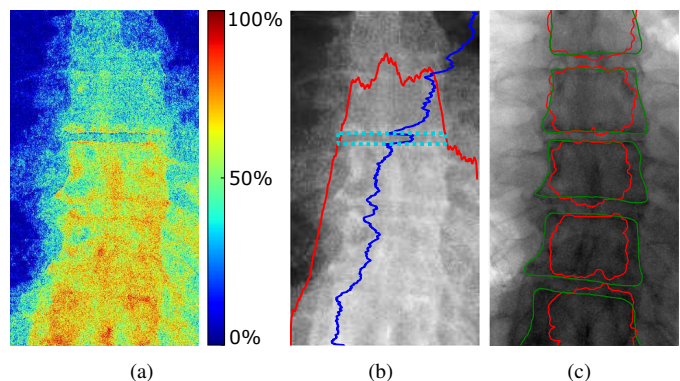


**Fig. 3:** (a) Probability map for bones: the probability ranges from blue to red, where blue denotes that the pixel is classified 0% as bone, and red denotes that the pixel is classified 100% as bone. (b) Inverted preprocessed image combined with the probability map with overlaid probability projections column-wise (red), row-wise (blue) and detected intervertebral disc (dotted light blue). (d) Overlay of the gold standard segmentation (green) and the segmentation result (red).

vertebrae detection. In combination with an active contours approach accurate and consistent results can be achieved.

#### DISCLAIMER

The methods and information presented in this paper are based on research and are not commercially available.

#### REFERENCES

- [1] P. Ponikowski, S. D. Anker, K. F. AlHabib, T. L. Cowie, Martin R. Force, S. Hu, T. Jaarsma, H. Krum, V. Rastogi, L. E. Rohde, U. C. Samal, H. Shimokawa, B. B. Siswanto, K. Sliwa, and G. Filippatos, "Heart failure: preventing disease and death worldwide," *ESC Heart Failure*, vol. 1, no. 1, pp. 4–25, August 2014.
- [2] P. Mountney, J. M. Behar, D. Toth, M. Panayiotou, S. Reiml, M.-P. Jolly, K. R., L. Zhang, A. Brost, C. A. Rinaldi, and K. Rhode, "A Planning and Guidance Platform for Cardiac Resynchronization Therapy," *IEEE Transactions on Medical Imaging*, June 2017.
- [3] R. Manzke, A. Bornstedt, A. Lutz, M. Schenderlein, V. Hombach, L. Binner, and V. Rasche, "Respiratory motion compensated overlay of surface models from cardiac MR on interventional x-ray fluoroscopy for guidance of cardiac resynchronization therapy procedures," in *SPIE Medical Imaging*. International Society for Optics and Photonics, February 2010, pp. 762 508–762 508.
- [4] T. Kurzendorfer, A. Brost, C. Forman, M. Schmidt, C. Tillmanns, and J. Hornegger, "Semi-Automatic Segmentation and Scar Quantification of the Left Ventricle in 3-D Late Gadolinium Enhanced MRI," in *32nd Annual Scientific Meeting of the European Society for Magnetic Resonance in Medicine and Biology*, October 2015, pp. 318–319.
- [5] P. Markelj, D. Tomaževič, B. Likar, and F. Pernuš, "A review of 3D/2D registration methods for image-guided interventions," *Medical Image Analysis*, vol. 16, no. 3, pp. 642–661, April 2012.
- [6] M. Kaiser, M. John, T. Heimann, T. Neumuth, and G. Rose, "Improvement of manual 2D/3D registration by decoupling the visual influence of the six degrees of freedom," in *11th International Symposium on Biomedical Imaging*. IEEE, April 2014, pp. 766–769.
- [7] R. De Silva, L. F. Gutiérrez, A. N. Raval, E. R. McVeigh, C. Ozturk, and R. J. Lederman, "X-Ray Fused With Magnetic Resonance Imaging (XFM) to Target Endomyocardial Injections: Validation of a Swine Model of Myocardial Infarction," *Circulation*, vol. 114, no. 22, pp. 2342–2350, November 2006.
- [8] D. Toth, M. Panayiotou, A. Brost, J. M. Behar, C. A. Rinaldi, K. S. Rhode, and P. Mountney, "Registration with Adjacent Anatomical Structures for Cardiac Resynchronization Therapy Guidance," in *International Workshop on Statistical Atlases and Computational Models of the Heart*. Springer, October 2016, pp. 127–134.
- [9] P. Fischer, T. Pohl, T. Köhler, A. Maier, and J. Hornegger, "A Robust Probabilistic Model for Motion Layer Separation in X-Ray Fluoroscopy," in *International Conference on Information Processing in Medical Imaging*. Springer, June 2015, pp. 288–299.
- [10] R. Szeliski, S. Avidan, and P. Anandan, "Layer extraction from multiple images containing reflections and transparency," in *IEEE Conference on Computer Vision and Pattern Recognition*, vol. 1. IEEE, June 2000, pp. 246–253.
- [11] A. Maier and R. Fahrig, *GPU Denoising for Computed Tomography*. CRC Press, October 2015.
- [12] R. M. Haralick, K. Shanmugam *et al.*, "Textural Features for Image Classification," *IEEE Transactions on Systems, Man, and Cybernetics*, vol. 3, no. 6, pp. 610–621, November 1973.
- [13] L. Breiman, "Random Forests," *Machine Learning*, vol. 45, no. 1, pp. 5–32, January 2001.
- [14] P. Marquez-Neila, L. Baumela, and L. Alvarez, "A morphological approach to curvature-based evolution of curves and surfaces," *IEEE Transactions on Pattern Analysis and Machine Intelligence*, vol. 36, no. 1, pp. 2–17, January 2014.